Nuclear Instruments and Methods in Physics Research B 295 (2013) 42–49

Contents lists available at SciVerse ScienceDirect

Nuclear Instruments and Methods in Physics Research B

journal homepage: www.elsevier.com/locate/nimb

Beyond filtered backprojection: A reconstruction software package for ion beam microtomography data

C. Habchi *, N. Gordillo, S. Bourret, Ph. Barberet, C. Jovet, Ph. Moretto, H. Seznec

Univ. Bordeaux, CENBG, UMR 5797, F-33170 Gradignan, France
CNRS, IN2P3, CENBG, UMR 5797, F-33170 Gradignan, France

ARTICLE INFO

Article history:
Received 22 June 2012
Received in revised form 6 September 2012
Available online 29 October 2012

Keywords:
Ion beam tomography
3D imaging
Filtered backprojection
MLEM
OSEM
ImageJ

ABSTRACT

A new version of the TomoRebuild data reduction software package is presented, for the reconstruction of scanning transmission ion microscopy tomography (STIMT) and particle induced X-ray emission tomography (PIXET) images. First, we present a state of the art of the reconstruction codes available for ion beam microtomography. The algorithm proposed here brings several advantages. It is a portable, multi-platform code, designed in C++ with well-separated classes for easier use and evolution. Data reduction is separated in different steps and the intermediate results may be checked if necessary. Although no additional graphic library or numerical tool is required to run the program as a command line, a user friendly interface was designed in Java, as an ImageJ plugin. All experimental and reconstruction parameters may be entered either through this plugin or directly in text format files. A simple standard format is proposed for the input of experimental data. Optional graphic applications using the ROOT interface may be used separately to display and fit energy spectra. Regarding the reconstruction process, the filtered backprojection (FBP) algorithm, already present in the previous version of the code, was optimized so that it is about 10 times as fast. In addition, Maximum Likelihood Expectation Maximization (MLEM) and its accelerated version Ordered Subsets Expectation Maximization (OSEM) algorithms were implemented. A detailed user guide in English is available. A reconstruction example of experimental data from a biological sample is given. It shows the capability of the code to reduce noise in the sinograms and to deal with incomplete data, which puts a new perspective on tomography using low number of projections or limited angle.

1. Introduction

1.1. Reconstruction of STIMT and PIXET data: a brief overview

The idea to use a focused light ion beam, typically protons or alpha particles of a few MeV, to probe samples a few hundred micrometers in diameter, was initially implemented by Pontau et al. [1], Fischer and Mühlbauer [2] and Schofield and Lefevre [3]. Scanning transmission ion microscopy tomography (STIMT) gives access to 3D morphology, with a typical spatial resolution of a few micrometers, or even down to a few hundred nanometers in the most favorable cases [4]. More precisely, STIMT provides 3D maps of the mass density (in g/cm^3) within the analyzed volume. In addition to STIMT, particle induced X-ray emission tomography (PIXET) can be carried out to map elemental content. Multielement detection and trace element sensitivity, down to a few ppm, are recognized as the main advantages of the PIXE technique.

From an historical point of view, the processing of ion beam microtomography data has been inspired by the codes developed for medical imaging, starting with the so-called "Donner library" [5]. Very few research groups have been involved in this development. For this reason, we would like to cite very early works, as they can be still considered as valuable approaches. First STIMT reconstruction codes were proposed, based on filtered backprojection (FBP) [1,2,6], ART or entropy maximum [7]. In these first studies, the choice of experimental conditions was discussed: incident beam energy, number of events, number of projections, etc. Optimal ways to process data were also presented, taking into account methodological studies already performed for conventional (2D) STIM: mean or median filtering of the transmitted energy, calculation of stopping power, effect of the filters, etc. Over the years, the comparison of these approaches led the authors to prefer the FBP code to reconstruct STIMT data, for its simplicity, reliability and speed. Two main aspects justify this choice: (i) the STIMT projections, measured by transmission, usually have very little noise

* Corresponding author at: Univ. Bordeaux, CENBG, UMR 5797, F-33170 Gradignan, France. Tel.: +33 5 57 12 08 98; fax: +33 5 57 12 08 01.
E-mail addresses: habchi@cenbg.in2p3.fr (C. Habchi), nuri.gordillo@gmail.com (N. Gordillo), bourret@cenbg.in2p3.fr (S. Bourret), barberet@cenbg.in2p3.fr (Ph. Barberet), jovet.c@gmail.com (C. Jovet), moretto@cenbg.in2p3.fr (Ph. Moretto), seznech@cenbg.in2p3.fr (H. Seznec).

0168-583X/$ - see front matter © 2012 Elsevier B.V. All rights reserved.
http://dx.doi.org/10.1016/j.nimb.2012.10.006

and (ii) the calculation of physical processes can usually be implemented following an analytical method. In this way, quantitative data can be obtained for thin samples [8].

The situation is more difficult for PIXET: the quantitative reconstruction of emission data requires an iterative algorithm, less sensitive to noise than FBP, and moreover able to take into account the attenuation of the emitted X-rays from their emission point to the detector. Pioneering studies were carried out by Schofield and Lefevre [3] and Antolak and Bench [9] using least squares methods derived from SPECT medical imaging (both from the Donner library). The second study improved the reconstruction process by combining the STIMT and PIXET reconstruction. In this way, local information about density is used to provide realistic attenuation factors, and reciprocally, local composition is used to calculate precise mass density. This more complete approach is required for the case of samples inhomogeneous in composition. A detailed study was carried out, where different sample compositions were compared, by increasing the levels or modifying the distribution of high Z elements in an organic matrix [9].

However, both approaches remained unsatisfactory in the sense that the X-ray detector was assumed point-like (zero solid angle). On the opposite, experimental conditions require that the detector should be as close as possible to the sample, in order to maximize counting statistics. The only code so far able to take into account the large solid angle required in real PIXET experiments was initially developed by Sakellariou et al. [10]. The DISRA program has remained the most complete code for the processing of STIMT/PIXET data, and has spread over the years in several research groups: Surrey [11], Leipzig [12], Bordeaux [13]. However, some restrictions inherent to the reconstruction method employed led some of them to explore other ways – although no complete solution has been reached so far. We would like here to summarize the main aspects of the reconstruction procedure in DISRA, to make clearer the origin of these limitations and how we could try to go beyond.

1.2. The Discrete Image Space Reconstruction Algorithm (DISRA)

The DISRA code was derived from a method initially developed for Positron Emission Tomography (PET). It is based on successive projections/backprojections of simulated data. To summarize, the starting tomogram (simulated 3D object) at zero order is guessed from the direct FBP of experimental projections (i.e. energy loss for STIMT, number of events for PIXET). This initial tomogram is then weighted, using an a priori global scaling factor. This factor is applied so that the content of every voxel of the initial tomogram can be of the same order of magnitude as the real physical parameter to be reconstructed (i.e. a mass density for STIMT, or a mass fraction for PIXET). Additional corrections (normalization, zeroing, etc.) are also brought, that we will not discuss here.

From this first "numerically guessed" tomogram, the iterations start: the physical processes of X-ray emission and attenuation are simulated, taking into account the detection solid angle specified by the user. A local correction factor is applied at every step, by comparing, voxel by voxel, the FBP of simulated data to the FBP of experimental projections, taken as a "reference reconstruction". To avoid noise amplification inherent to FBP, the originality of DISRA is that every voxel value is limited by a bandwidth $\Delta D_{(i)}$ at the ith iteration. This limitation is performed in a smart way, as the bandwidth is reduced at each iteration, since the voxel values are getting closer to convergence. More precisely, it follows the formula:

$$\Delta D_{(i)} = d \times 2^{-(2+i)}$$

In this formula, d is an arbitrary numerical factor different for STIMT and PIXET data. The convergence is reached when the simulated data are found to be close enough to the experimental ones.

1.3. Current limitations and prospects

DISRA has been proven to generate accurate mass density and mass fractions results, both on simulated "phantom" objects and on experimental data [14], at least for inorganic samples presenting a good density contrast and high X-ray yields. However, for less contrasted objects, such as biological samples, limitations of DISRA may appear. From an experimental point of view, the duration of PIXET data acquisition may be of a few hours per slice, depending on the number of pixels, number of projections and element concentration. To give an example, for isolated cells or for small organisms such as the nematode presented here, it typically takes about 1–2 h beam time to map the mineral content (typical concentration about a few per thousand in dry mass). To give a comparison, a full 3D (128 slices) STIMT experiment may take about the same time. In these conditions, both experiment duration and sample damage would be prohibitive to perform 3D PIXET. Instead, it appears advisable to probe isolated PIXET slices, in regions of interest selected from 3D STIMT reconstruction. A modification of the DISRA code was introduced to handle this configuration [13].

A second difficulty in DISRA is the arbitrary numerical factor used for discretization. The default values imposed in the code can turn out to be inappropriate in certain conditions, such as for low mass fractions. In these conditions the iterations are prohibitively slowed down and the source code has to be modified "manually", according to the considered sample [15].

We could see a last obstacle to the application of DISRA for biological studies, which is inherent to the FBP process used for reconstruction. From an experimental point of view, the sample is mounted as freestanding, attaching to the top of the rotation axis. To prepare the sample this way can turn out to be a rather difficult task for fragile biological samples, such as isolated cells. A more convenient option would be to probe cells deposited on a 2D substrate, using limited angle tomography, as it is done for electron tomography for instance [16]. However, because of the FBP algorithm implemented at each iteration, this possibility cannot be handled by DISRA at this stage.

An innovative approach was proposed by Andrea et al. [17] for limited angle tomography of single cells, over an angular range of 120°. In this study, the missing STIMT projections, over the 60° angle range not covered by the beam, were interpolated using a back and forth numerical guess of the complete sinogram, based on a FBP method. Noise amplification in the image outside the sample was eliminated by image processing. Qualitative PIXET reconstruction was performed the same way. Satisfactory images were obtained. However, because FBP is intrinsically an analytical method, we believe that other algorithms should be considered as more promising options for limited angle tomography.

For all these reasons, we would like here to propose an alternative to FBP for the reconstruction of low-contrast objects such as biological samples. To tackle the full problem of the reconstruction of PIXET data as precisely as DISRA is able to do it (when all conditions are fulfilled for the convergence to be reached) will definitely take a long effort. We propose here a new development of the TomoRebuild data reduction software package [18], able to perform quantitative STIMT and qualitative PIXET reconstruction. To broaden the reconstruction possibilities, in addition to FBP, two iterative reconstruction methods are proposed, able to tackle the problems of noise amplification – even for a small number of projections – and limited range tomography. This development was made keeping as a main goals ease of use and portability, whatever the operating system and experimental conditions. Below, we present an example of experimental data reduction for a biological sample. However, the software package is more general and could be implemented for any type of sample.

2. Experimental procedure

2.1. Sample preparation

Tomography experiments were carried out on small organisms, *Caenorhabditis elegans* (*C. elegans*), extensively used as a model for biological studies (http://www.wormbook.org/). *C. elegans* is a small worm, from the nematode phylum, about 1 mm in length, which usually lives in temperate soils, and that is widely grown in cell culture laboratories. For these tomography experiments, *C. elegans* were cultured in typical conditions, at room temperature (19 °C) on Nematode Growth Medium agar, with a bacterial lawn of *Escherichia coli* OP50.

Worms were picked up by aspiration into glass microtubes, used as sample support. The samples were cryofixed and freeze-dried to permit under vacuum analysis. Only the upper part of the worm, remaining outside the microtube, was analyzed.

2.2. Nanobeam line

STIMT and PIXET experiments were carried out at the so called "nanobeam" line, recently designed at the AIFIRA facility (Applications Interdisciplinaires des Faisceaux d'Ions en Région Aquitaine) of Bordeaux. The facility is based on a 3.5 MV HVEE (High Voltage Engineering Europa, Netherlands) Singletron™ particle accelerator, delivering light ion beams (protons, deutons or alphas). The ion beam is focused using a doublet–triplet of quadrupolar magnetic lenses provided by Oxford Microbeams Ltd. An exhaustive description may be found in a previous publication [19].

The analysis chamber was specifically designed for fine observation and positioning of biological samples. Three microscope objectives (4×, 10×, 20×) can be positioned in the analysis chamber to select regions of interest on the sample. A universal motion controller (XPS, Newport™), addressed via an Ethernet connection, allows to adjust the position of the sample stage, of the detectors and of the objectives. For tomography, the sample holder is placed on a goniometer with a four-axis movement designed to permit a precise alignment of the sample along the rotation axis, with an accuracy of 1° in tilt and of 1 μm in translation. A precise description of the chamber and of the alignment procedure may be found in a previous publication [20].

In STIMT configuration, the beam spot on the sample is typically ~0.3 μm large [19]. The beam intensity is of a few thousand ions per second, i.e. less than 1 femtoampere. Such a low intensity prevents from any beam damage of the sample, like any distortion or shrinkage. In this way, STIMT is considered as non-destructive, at least from a macroscopic point of view. The transmitted beam is measured directly "on axis", in a passivated implanted planar silicon detector (Canberra PIPS detector, 25 mm^2, 12 keV energy resolution).

For PIXET, higher beam intensity is used, to provide sufficient X-ray emission rates. In this configuration, the beam spot on sample is about 1 μm wide, with a typical beam intensity of a few hundred picoamperes. X-rays are detected using a Si(Li) scintillator (e2v Sirius detector, 80 mm^2, 148 eV resolution for the Mn K_α line) placed at 135° backwards.

2.3. Acquisition procedure

The tomography experiments were carried out using a 1.5 MeV proton beam. For STIMT, the energy has to be chosen high enough for the beam to go through the sample, but also low enough to optimize density contrast. The acquisition procedure for STIMT and PIXET tomography is automatically controlled, coupled to the sample stage and detector holders and to the beam positioning systems. For each projection, events are recorded in a binary list file containing the information required for data reduction, i.e. the position of the beam, the measured energy (channel) and the considered detector.

Acquisition duration depend on the size of the region of interest and on the expected spatial resolution. We give here the conditions applied for the sample displayed hereafter. The beam was scanned two-dimensionally over the sample at every projection (i.e. each angular position of the sample) over a rectangular area of 100 μm in width × 200 μm in height. The beam was moved point by point, following a rectangular grid 128 pixels in width and 255 pixels in height. In this way, 255 horizontal STIMT slices were probed, each one being reconstructed over 128 × 128 pixels. The resulting spatial resolution was therefore limited by the scan parameters, to 0.79 μm/pixel both in the horizontal and vertical directions.

In order to minimize any damage to the sample, and also to the transmission detector, even at so low intensity, several high-speed scans were repeated at each projection, instead of one single scan. For this experiment, 30 scans were performed at 200 μs per point. The detector was moved typically every 20 projections to avoid local damage on the small area exposed to the focused beam, which would be noticeable as a resulting energy drift in the transmitted energy spectrum. The detector region that will be exposed to the beam is checked before starting the tomography experiment, in order to avoid hitting any surface defect during acquisition. In this way, the detector damage mentioned in paragraph 3.3 and visible in Fig. 1 remains very exceptional. The sample was rotated of 1.8° after each projection, so that a total of 100 projections was collected over 180°. In these conditions, the duration of the STIMT experiment was about 5 h.

For PIXET, the duration of acquisition, typically 2 h per slice for these samples, prevents a full 3D exploration of the volume. Therefore, several slices of interest were selected from the STIMT reconstruction and from conventional 2D PIXE analysis of this region. This first quick two-dimensional PIXE scan prior to tomography does not lead to a visible damage of the sample, thanks to the low beam intensity (about 300 pA in the following example) and high scan speed. The experimental conditions for PIXET were similar to STIMT, except for: (i) the scan shape, which is a single horizontal line in order to probe an individual horizontal slice and (ii) the higher number of scans per projection, about 3000 scans, in order to improve counting statistics for X-ray emission. As for STIMT, the PIXET experiment was carried out using 100 projections over 180° only. We did not choose a full 360° rotation, with the aim of preserving spatial resolution, as the sample was thin enough to avoid a drastic attenuation of the emitted X-rays. We estimated the X-ray attenuation by using a semi-empirical calculation proposed by Henke et al. [21] and implemented by the Center for X-ray Optics of the Lawrence Berkeley National Laboratory (http://henke.lbl.gov/optical_constants). The maximal thickness of the sample presented below was obtained from the STIMT sinogram: 2.8 mg/cm^2. This value corresponds to the thickest diameter of the worm within the analyzed volume. In this worst case trajectory, the emitted X-rays (K_α lines) would undergo an attenuation of about 38% for phosphorus, 28% for sulfur and 7.8% for calcium.

3. Data reduction software package

3.1. Main features

This new version of the TomoRebuild reconstruction software package was developed keeping in mind the wide variety of acquisition systems, experimental conditions and operating systems that may occur for ion beam tomography. The code is written in

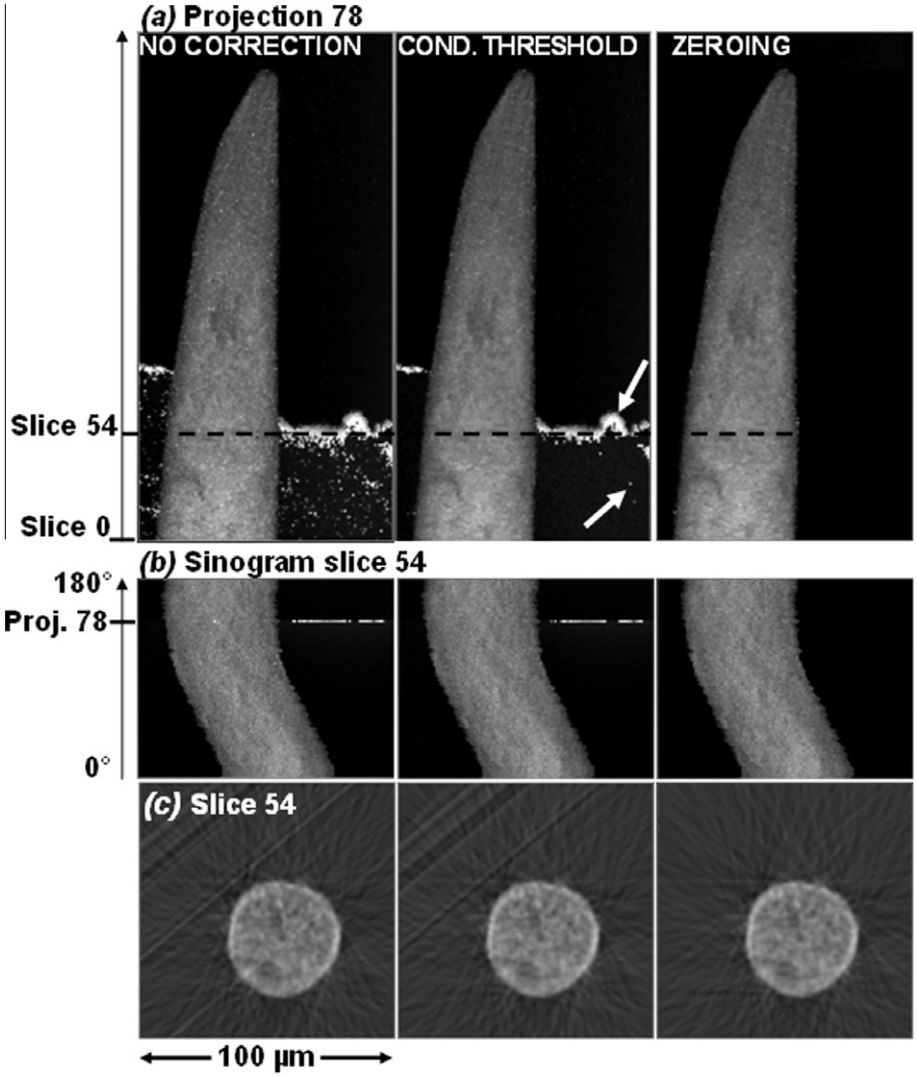

Fig. 1. Successive correction steps of experimental data: conditional thresholding and zeroing mask applied to the projections (a) and, in an equivalent way, to the sinograms (b). Slice 54 was chosen as an example to display the effect of the corrections in the FBP reconstruction (c). The position of this slice is indicated by a horizontal dashed line in (a). Reciprocally, the position of projection 78 is mentioned in the sinogram (b). Images are displayed using a linear gray scale ranging from 0 (black) to the maximal thickness (3.4 mg/cm^2, white) for (a) and (b). Tomographic slices (c) are the direct result of FPB using a Hann filter with 0.5π frequency cut-off, without any further filtering or thresholding after reconstruction. The linear gray scale ranges from the minimal reconstructed value of mass density (-0.29 g/cm^3, black) to the maximal value (1.1 g/cm^3, white). Negative density values were here intentionally kept to reveal noise outside the sample.

C++, with a modular structure in separated classes, which makes it easier to use and to modify whatever the operating system. The reconstruction is decomposed in different steps. The result of each step may be checked before going to the next one, and, if necessary, optional correction procedures may be applied to the data. To save memory space and increase computational speed, intermediate result files are generated in binary format, but with a possible translation in ASCII, if required by the user for checking.

All experimental parameters are defined through parameter files written in simple text format – to avoid any re-compilation of the code. Although every step may be executed as a simple command line, a multi-platform user-friendly graphic interface is proposed to facilitate parameter input and code execution. This interface was developed as a portable Java plugin in ImageJ, which is a public domain, open-source Java-based image processing program developed at the National Institutes of Health (http://rsb-web.nih.gov/ij/). It uses the same text parameter files as the command line version. A detailed user guide in English is provided to use the code, with or without graphic interface.

The reconstruction is performed without requiring the installation of any graphic library or numerical tool. Sinograms and final reconstructed images are generated in usual binary formats that can be read either using the Amira® graphic library (http://www.amira.com) or public domain softwares, such as ImageJ. Optional graphic applications using the ROOT interface may be used to display and fit energy spectra for any projection(s). However these optional programs were intentionally kept separated from the TomoRebuild code, to avoid any dependence to non-standard external libraries.

The FBP code was optimized so that the duration was reduced by a factor of about 10 compared to the previous version. For instance, the FBP reconstruction of the example hereafter (255 slices, 128×128 pixels, 100 projections) takes less than 2 min on a conventional x86 double core Pentium D PC, 1024 Mb random access memory, using the Window XP operating system.

3.2. Data input

The starting point for the reconstruction is the experimental data file. A standard format was defined, providing the information required: the measured energy (channel number), the horizontal and vertical position of the beam (pixel numbers), the projection

Table 1
Average density of a SiC reference sample, as calculated form a region of interest of about 500 voxels. The given uncertainty only corresponds to the standard deviation.

	Results in 10^2 g/cm^3	
	FBP	MLEM
Slice 1	268.4 ± 4.5	269.8 ± 4.6
Slice 2	268.5 ± 5.7	269.7 ± 5.0
Slice 3	270.6 ± 3.6	272.4 ± 4.4
Average	269.2 ± 2.7	270.6 ± 2.7
Reference value 273–277		

number. Only linear (one slice) or rectangular scans can be interpreted. Data do not have to be centered along a rotation axis that should be perfectly vertical and positioned in the middle of the sinogram.

3.3. Correction of sinograms

The correction procedures already implemented in the previous version of TomoRebuild for STIMT have been kept and optimized. The presence of spurious events, due to pile up, electronic noise, ion scattering inside the beamline for instance, leads to a random "speckle" noise in the sinogram. To correct for these abnormal events, several corrections are implemented. First, a high and low thresholds are applied on the energy spectrum to discard respectively pile up and electronic noise. In a second step, median (or mean) filtering is implemented to get the most probable value of the transmitted energy per pixel. This filtering is usually very efficient, but, if necessary, a third step can be used to get rid of the residual noise that may occur: each pixel is compared to its immediate neighbors. A conditional threshold is applied, in order to maintain the spatial resolution of the image whilst achieving efficient correction. A pixel is corrected only if it is considered as "non-reliable", i.e. if the number of events collected a that position is lower than a user defined threshold, and if the difference with its immediate neighbors is higher than a user defined threshold.

An additional correction is proposed in this new version, to clean spurious events that may remain outside the sample in the STIMT and PIXET sinograms. The edges of the sample, automatically determined from the STIMT sinogram, are used to define a mask. All pixels outside this mask may be set to zero in the STIMT and/or PIXET sinogram.

In Fig. 1, we took advantage of an unusual experimental problem of detector damage, which occurred during projection 78 of the sample presented hereafter, and that we here intentionally kept during acquisition, to visualize the effect of the different correction procedures. This local damage is visible as white spots in the bottom part of projection 78 (Fig. 1a). Most of these are isolated pixels, which can be removed by the first step of conditional thresholding correction. However, non-isolated pixels, in a ribbon-like area, as well as a few particular isolated pixels having a number of events higher than the user defined confidence threshold (see arrows) remained. In the second step (right hand image), these anomalous pixels were zeroed by the edge detection mask applied to the projection data. In an equivalent way, these corrections are also visible in the sinogram of slice 54, chosen as an example (Fig. 1b). The consequence in the FBP reconstruction is displayed in Fig. 1c. Anomalous white spots in the projections give raise to characteristic streaking artifacts in the reconstructed slice. They disappear in the right hand image, with the zeroing procedure. The remaining streaks along the edges of the sample in this image are inherent to the FBP itself.

3.4. Determination of rotation axis

Rotation centers are calculated for each slice independently. It should be noted that the procedure – based on the motion of the center of mass during sample rotation – gives precise results for STIMT only. However, it proves to be robust enough to be used also for PIXET, at least as a first guess, especially for smooth-shaped biological samples. A linear regression is implemented to determine the best rotation axis. The FBP reconstruction is then performed for each slice using these positions and does not require a re-alignment of the sinogram in the middle of the image, nor to have a perfectly vertical rotation axis.

3.5. Reconstruction algorithm

Although FBP can be considered as a fast and reliable method for low noise data such as STIMT, inherent artifacts, especially along high frequency edges, reduces the quality of reconstructed images (Fig. 1c). For low contrasted data such as biological samples, interpretation of images would be easier with a less noisy reconstruction. To address this problem, two iterative statistical algorithms, widely used for PET and SPECT medical imaging, were implemented: Maximum Likelihood Expectation Maximization (MLEM) and its accelerated version Ordered Subsets Expectation Maximization (OSEM) [22]. The reconstruction is also performed slice by slice, using the precise position of the rotation center. However the calculation of the probability matrix, which is the core and most time consuming part of the code, was optimized so that it is not performed for every slice, but only if the rotation center differs from more than ±0.5 pixel. In this way, a reconstruction in the conditions described above requires about 12 min for MLEM and 5 min for OSEM. To our knowledge, this is the first time

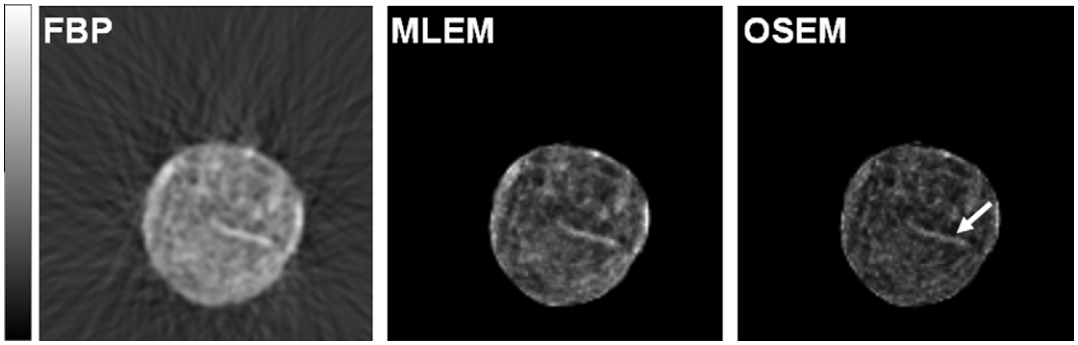

Fig. 2. Comparison of FBP, MLEM and OSEM reconstructions for slice 0 of the *C. elegans* sample. Conditions of reconstruction: FBP using Hann filter with 0.5π frequency cut-off; MLEM 32 iterations; OSEM 16 subsets and four iterations. The bar shaped structure (arrow) was identified as the lumen of intestine, which collapsed during sample freeze-drying.

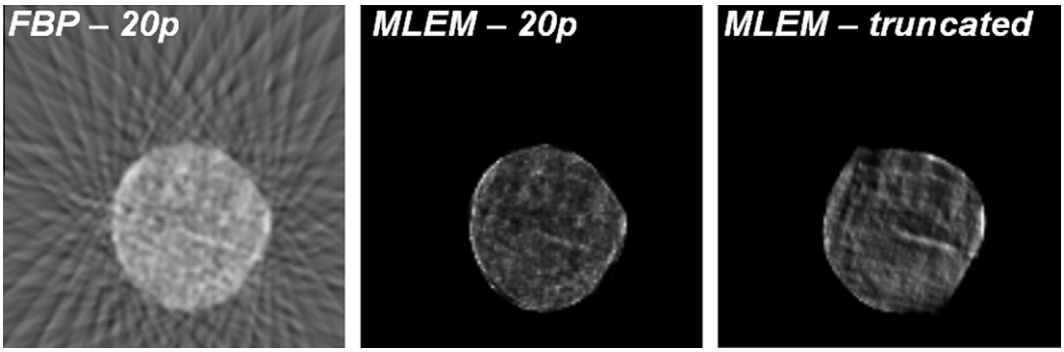

Fig. 3. Reconstruction from incomplete data sets of slice 0 of the *C. elegans* sample. *Left and middle:* FBP and MLEM results from 20 projections over 180°. *Right:* MLEM result from 70 projections over the [0°; 124, 2°] angle range. The same reconstruction conditions as in Fig. 2 were applied.

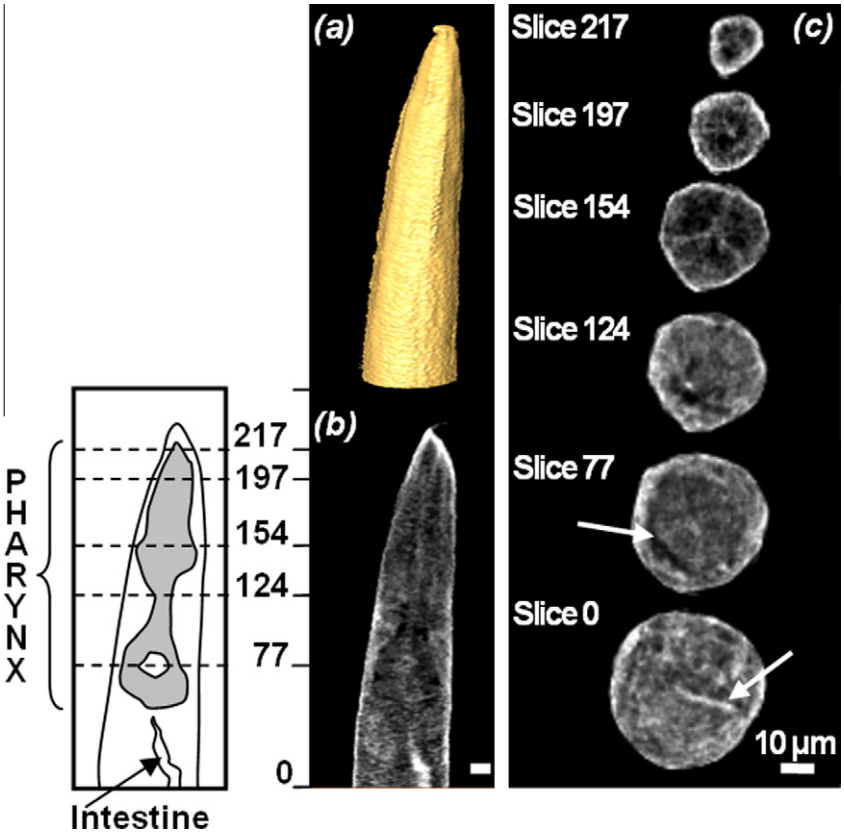

Fig. 4. Three-dimensional structure of the upper part of the *C. elegans* sample, as obtained from the MLEM reconstruction of 255 STIMT slices: 3D view of the outer surface of the worm (a); longitudinal slice through the reconstructed volume and its corresponding sketch (b); a few horizontal slices (c). The vertical position of the slices is indicated on the left. Reconstructed mass density values were coded on a linear gray scale ranging from 0.01 (black) to 0.9 g/cm^3 (white), except for slice 217, which presents denser regions, ranging from 0.25 to 1.1 g/cm^3.

that the OSEM code has been implemented for ion beam microtomography and, from a broader perspective, one of the rare OSEM freeware versions available. Our version was based upon the calculation of probability matrix described by Loudos [23] for SPECT.

Quantitative calculation of mass density, based on the determination of the sample stopping power, is achieved by assuming that samples have a uniform composition of major elements, as it is usually the case for biological samples. This calculation was checked for FBP and MLEM using reference specimens such as described in a previous publication [18]. Similar results were obtained for both methods. As an example, we present in Table 1 the STIMT results from three tomographic slices across a microcomposite sample, used as a reference specimen, containing a SiC fiber of known density [18]. The calculated values of mass density are in good agreement with the reference value. However, we did not manage to get quantitative STIMT reconstructions from OSEM. Moreover, OSEM images usually appear as slightly less contrasted than MLEM. For these reasons, we would recommend to Tomorebuild users to rather use OSEM as a quick test method to get first images to check and adjust all reconstruction parameters, and then use MLEM to obtain the final reconstruction.

The direct result of FBP, MLEM and OSEM is compared in Fig. 2 on a particular slice of the *C. elegans* sample. Intentionally, no additional smoothing or thresholding was brought, to emphasize the difference between the reconstructed images. Noise outside the specimen almost disappears and the edges of the structures are

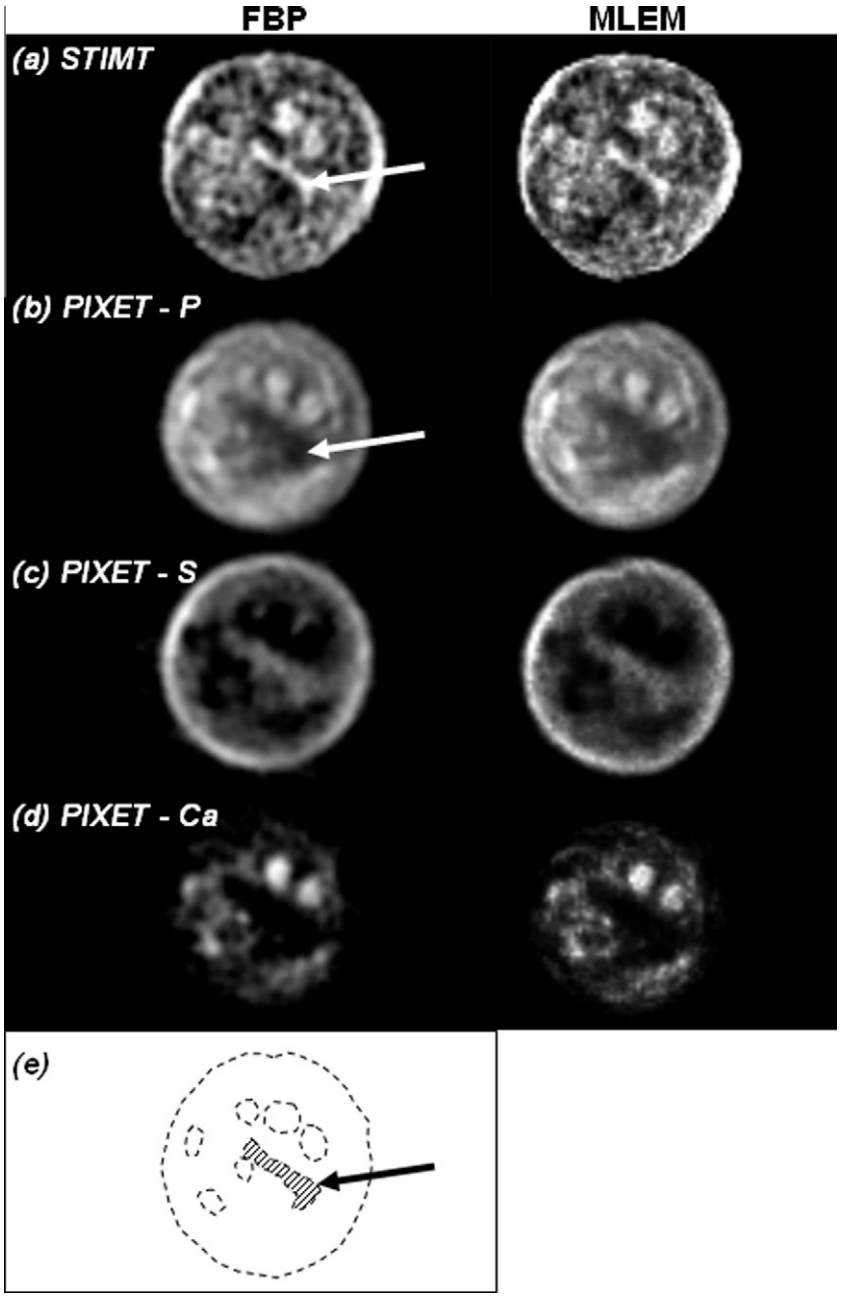

Fig. 5. Tomographic reconstructions corresponding to the STIMT slice number 23 (*a*), as obtained from FBP (*left*) and MLEM (*right*). The mass density STIMT map was represented using a linear gray scale ranging from 0.09 (black) to 0.9 g/cm^3 (white) for both methods. Qualitative element distributions are presented below (*b*–*d*). Several high-density spots, noticeable in the STIMT map and also visible especially in the PIXET-Phosphorus map (*b*), were schematically represented in (e) to guide the eye. As in Fig. 4, the intestine can be identified from the STIMT map (arrow) and was represented by a hatched area in (e).

more visible in MLEM and OSEM compared to FBP. Beyond image quality, iterative statistical methods present the capability to generate reconstructed images using less projection data than FBP. This advantage was put forward several years ago for ion beam tomography by Ng et al. [24], showing the reconstruction of a 60×60 pixels simple shaped object from only eight projections. However, to our knowledge, this code has never been implemented elsewhere for STIMT or PIXET. Fig. 3 shows the results on the same 128×128 pixels slice as Fig. 2, obtained from only 20 projections over 180°, using FBP and MLEM. The FBP reconstruction is completely blurred by the too sparse sampling, whereas MLEM appears as more robust.

Another intrinsic limitation of FBP, to require projection angles over at least 180°, is not necessary for iterative statistical methods. An example of MLEM reconstruction from truncated data composed of 70 projections over the [0°; 124, 2°] angle range is displayed in Fig. 3. As discussed above, this method could facilitate the reconstruction of limited angle tomography data and could constitute an alternative to the option proposed by Andrea et al. [17].

4. Results and discussion

4.1. 3D STIMT reconstruction

The 3D structure of the *C. elegans* sample described above was obtained from STIMT. Fig. 4 displays the reconstruction of the head,

down to the beginning of intestine, as obtained from 255 experimental slices, reconstructed using the MLEM algorithm. In Fig. 4a, the surface obtained from the voxels having a density value close to zero, characteristic from the limit between the sample and surrounding vacuum, was selected, to show the outer surface of the worm. A longitudinal slice across the sample was selected to show the inner structure of pharynx (Fig. 4b), as indicated in the sketch. Specific areas of interest can be also identified in the horizontal slices Fig. 4c: the mouth (slice 217), the beginning of digestive tract (center of slice 197), the characteristic three pointed star shape of larynx (slice 154), the rounded shape of the lower part of larynx (arrow in slice 77), the beginning of intestine, that collapsed during the freeze drying step (arrow in slice 0).

4.2. Elemental distributions from PIXET

Isolated PIXET slices were probed in regions of interest within the STIMT volume. Tomographic images were reconstructed using the FBP, MLEM and OSEM algorithms, now available in this new version of TomoRebuild, which produced, as expected, similar distributions. An example of FBP and MLEM reconstructions corresponding to the STIMT slice 23 (Fig. 5a) (keeping the same numbering as in Fig. 4) is presented in Fig. 5. The intestine can be recognized from the STIMT map as a high-density region (arrow). Distributions of three elements, phosphorus, sulfur and calcium (Fig. 5b–d) were reconstructed by selecting the corresponding K lines on the PIXET energy spectrum. It should be noted that these reconstructions are only qualitative, in the sense that they have been directly obtained from the X-ray yield emitted from the slice.

A schematic view of the most noticeable features appearing in the P reconstruction and also visible in the STIMT image (Fig. 5a and b) was represented in Fig 5e to guide the eye. The arrow in the tomographic slices and in the schematic representation indicates the intestine. A biological interpretation of such images is going out of the scope of this paper. However, the images presented here show the capability of the reconstruction algorithm to produce elemental distributions from PIXET data.

5. Conclusion and outlook

This new version of TomoRebuild has been optimized for a rapid and easy data processing of STIMT and PIXET experiments. Although it could be used for any type of sample, it appears as particularly suited to biological samples for two main reasons: (i) the noise correction procedures proposed for sinograms improve image quality, which is especially important for low contrast images and (ii) the MLEM and OSEM methods open a wider possibility to reconstruct data from limited angular range or from a small number of projections.

The development of fully quantitative PIXET reconstruction, according to a method as complete as the DISRA algorithm, including especially the modeling of X-ray absorption in a large solid angle, would constitute a long-term evolution of this software package.

Acknowledgements

The authors are grateful to Laurent Daudin, Stéphanie Sorieul, Philippe Alfaurt, Franck Delalée and Laurent Sérani, Centre d'Etudes Nucléaires de Bordeaux Gradignan, France, for their support in the technical developments on the beamline. We would also like to thank George Loudos, Athens School of Technological Applications, Greece, and Benoît Recur, Laboratoire Bordelais de Recherche en Informatique, Talence, France, for fruitful help in implementing the OSEM code. We are grateful to Denis Dupuy, Institut Europeen de Chimie et Biologie, Pessac, France, for providing the *C. elegans* strain to our laboratory.

This work has been partly supported by the European Community as an Integrating Activity "Support of Public and Industrial Research Using Ion Beam Technology (SPIRIT)" under EC contract no. 227012. *C. elegans* experiments have been carried out in the frame of the ANR Program: "Contaminants, Ecosystèmes, Santé 2010", in the TITANIUMS project.

References

[1] A.E. Pontau, A.J. Antolak, D.H. Morse, A.A. Ver Berkmoes, J.M. Brase, D.W. Heikkinen, H.E. Martz, I.D. Proctor, Ion microbeam tomography, Nucl. Instr. Res. B 40 (41) (1989) 646–650.
[2] B.E. Fischer, C. Mühlbauer, Microtomography by heavy ions, Nucl. Instr. Res. B 47 (1990) 271–282.
[3] R.M.S. Schofield, H.W. Lefevre, PIXE-STIM microtomography: zinc and manganese concentrations in a scorpion stinger, Nucl. Instr. Res. B 72 (1992) 104–110.
[4] T. Andrea, M. Rothermel, T. Butz, T. Reinert, The improved STIM tomography set-up at LIPSION: three dimensional reconstruction of biological samples, Nucl. Instr. Res. B 267 (12–13) (2009) 2098–2102.
[5] R.H. Huesman, G.T. Gullberg, W.L. Greenberg, T.F. Budinger, RECLBL library users manual: donner algorithms for reconstruction tomography, Pub. 214, Lawrence Berkeley Laboratory, 1977.
[6] A.E. Pontau, A.J. Antolak, D.H. Morse, Some practical considerations for ion microtomography, Nucl. Instr. Res. B 45 (1990) 503–507.
[7] G. Bench, K.A. Nugent, M. Cholewa, A. Saint, G.J.F. Legge, Submicron STIM tomography reconstruction techniques, Nucl. Instr. Res. B 54 (1991) 390–396.
[8] C. Michelet-Habchi, S. Incerti, P. Aguer, Ph. Barberet, E. Gontier, T. Guinefolleau, Ph. Moretto, A. Pouthier, T. Pouthier, R.W. Smith, 3D imaging of microscopic structures using a proton beam, IEEE Trans. Nucl. Sci. 52 (3) (2005) 612–617.
[9] A.J. Antolak, G.S. Bench, PIXE tomography of samples with inhomogeneous elemental composition, Nucl. Instr. Res. B 88 (1994) 297–307.
[10] A. Sakellariou, M. Cholewa, A. Saint, G.J.F. Legge, An accurate reconstruction algorithm for tomography experiments that involve complex probe–sample interactions, Meas. Sci. Technol. 8 (1997) 746–758.
[11] D. Beasley, N.M. Spyrou, 3D quantitative elemental mapping using simultaneous proton induced X-ray emission tomography and scanning transmission ion microscopy tomography, Nucl. Instr. Res. B 264 (2) (2007) 323–328.
[12] M. Rothermel, T. Reinert, T. Andrea, T. Butz, First results on ion microtomography at LIPSION, Nucl. Instr. Res. B 268 (11–12) (2010) 2001–2005.
[13] C. Habchi, D.T. Nguyen, Ph. Barberet, S. Incerti, Ph. Moretto, A. Sakellariou, H. Seznec, Reconstruction of 3D ion beam micro-tomography data for applications in Cell Biology, Nucl. Instr. Res. B 267 (12–13) (2009) 2107–2112.
[14] A. Sakellariou, STIM and PIXE tomography, PhD thesis, School of Physics, University of Melbourne, 2002.
[15] D.T. Nguyen, Développement d'algorithmes de reconstruction tomographique pour l'analyse PIXE d'échantillons biologiques, PhD thesis, University of Bordeaux 1, n3589, 2008.
[16] D. Vanhecke, S. Asano, Z. Kochovski, R. Fernandez-Busnadiego, N. Schrod, W. Baumeister, V. Lučić, Cryo-electron tomography: methodology, developments and biological applications, J. Microsc. 242 (3) (2011) 221–227.
[17] T. Andrea, M. Rothermel, R. Werner, T. Butz, T. Reinert, Limited angle STIM and PIXE tomography of single cells, Nucl. Instr. Res. B 268 (11–12) (2010) 1884–1888.
[18] C. Michelet-Habchi, S. Incerti, P. Aguer, Ph. Barberet, E. Gontier, K. Grente, Ph. Moretto, D.T. Nguyen, A. Pouthier, T. Pouthier, F. Rebillat, R.W. Smith, TomoRebuild: a new data reduction software package for scanning transmission ion microscopy tomography, Nucl. Instr. Res. B 231 (1–4) (2005) 142–148.
[19] Ph. Barberet, L. Daudin, N. Gordillo, S. Sorieul, M. Simon, H. Seznec, I. Idarraga, S. Incerti, A. Balana, Ph. Moretto, First results obtained using the CENBG nanobeam line: performances and applications, Nucl. Instr. Res. B 269 (20) (2011) 2163–2167.
[20] N. Gordillo, C. Habchi, L. Daudin, A. Sakellariou, F. Delalée, Ph. Barberet, S. Incerti, H. Seznec, Ph. Moretto, Technical developments for computed tomography on the CENBG nanobeam line, Nucl. Instr. Res. B 269 (20) (2011) 2206–2209.
[21] L. Henke, E.M. Gullikson, J.C. Davis, X-Ray interactions: photoabsorption, scattering, transmission, and reflection at $E = 50–30{,}000$ eV, $Z = 1–92$, At. Data Nucl. Data Tables 54 (2) (1993) 181–342.
[22] H.M. Hudson, R.S. Larkin, Accelerated image reconstruction using ordered subsets of projection data, IEEE Trans. Med. Imaging 13 (4) (1994) 601–609.
[23] G.K. Loudos, An efficient analytical calculation of probability matrix in 2D SPECT, Comput. Med. Imaging Graph. 32 (2) (2008) 83–94.
[24] Y.K. Ng, I. Orlic, S.C. Liew, K.K. Loh, S.M. Tang, T. Osipowicz, F. Watt, A PIXE micro-tomography experiment using MLEM algorithm, Nucl. Instr. Res. B 130 (1–4) (1997) 109–112.